

## 回音壁微腔激光器电老化试验及寿命分析

樊碳润<sup>1,2</sup>, 肖金龙<sup>2,3\*</sup>, 杨跃德<sup>2,3</sup>, 郝友增<sup>2,3</sup>, 黄勇涛<sup>2,3</sup>, 黄永箴<sup>1,2,3</sup>

<sup>1</sup>中国科学院大学微电子学院, 北京 100049;

<sup>2</sup>中国科学院半导体研究所集成光电子学国家重点实验室, 北京 100083;

<sup>3</sup>中国科学院大学材料科学与光电工程中心, 北京 100049

**摘要** 为了考察深刻蚀结构的回音壁模式半导体微腔激光器的寿命, 采用恒电流模式对 InGaAsP/InP 多量子阱耦合双圆微腔激光器进行了电老化试验, 电流应力为 100 mA, 老化总时长为 1400 h。对比了电老化试验前期、中期和后期器件的输出光谱和功率-电压-电流( $P$ - $V$ - $I$ )特性, 以器件稳定工作的电老化中期为例分析了器件的性能。分析了输出功率和阈值电流随时间的变化情况, 判断出在电老化试验期间器件退化模式始终为渐进模式。以器件输出功率降到初始值的 50% 作为失效判据标准, 在 100 mA 电流下, 器件的寿命约为 1200 h。

**关键词** 激光器; 微腔; 可靠性; 电老化试验; 电流应力; 寿命

中图分类号 TN248.4

文献标志码 A

doi: 10.3788/CJL202249.0601001

### 1 引言

半导体激光器在工作中会因为灾难性光学损伤、腔面氧化、电极键合老化等而发生退化直至失效, 其所在应用系统的可靠性受到影响<sup>[1-5]</sup>。电老化试验是评价半导体激光器寿命的常用方法, 分为恒功率和恒电流两种模式<sup>[6]</sup>。恒功率模式更接近激光器的实际应用情况, 但为了维持恒功率, 就需要建立闭环控制系统, 这使得试验系统较为复杂。恒电流模式实施起来相对较为简单, 只需间隔几个小时或几天进行功率测量。

回音壁模式(WGM)半导体微腔激光器因具有体积小、品质因子高和易于集成等优点, 在片上光子集成、微波光子学等领域中有广泛的应用<sup>[7-9]</sup>。为了实现光线在腔体内部的全反射, WGM 微腔选用深刻蚀结构, 刻蚀深度超过有源区, 这给包括有源区在内的刻蚀界面带来大量的缺陷和损伤, 特别是非辐射复合中心。WGM 微腔刻蚀界面处的光场强度较高, 会加速缺陷和损伤的发展。这种异于传统脊形波导半导体激光器的深刻蚀结构会加速 WGM 微

腔激光器的退化, 因此针对 WGM 微腔激光器的可靠性研究和寿命分析变得十分必要。

Han 等<sup>[10]</sup>在 85 °C 下对平面掩埋型异质结构的 InGaAsP/InP 量子阱法布里珀罗激光器进行了 2100 h 的恒功率加速老化试验, 并对其寿命进行了估计。Huang<sup>[11]</sup>通过对掩埋异质结构的激光器进行高温加速老化试验, 对半导体激光器可靠性的外推方法进行了验证。马骁宇课题组使用电致发光技术对分离限制异质结构的激光器进行了失效模式分析<sup>[12]</sup>, 对脊形波导结构的高功率激光器进行了恒电流加速老化试验<sup>[13]</sup>。

为了研究深刻蚀结构的 WGM 半导体微腔激光器在最佳工作状态下的寿命, 本文选取恒电流模式对由 InGaAsP/InP 多量子阱外延片制作的耦合双圆 WGM 微腔激光器进行了电老化试验, 分析了其老化前期、中期和后期的性能, 得到了输出功率和阈值电流随时间的变化曲线, 分析了曲线出现异常变化的原因, 并根据其变化趋势判断器件在电老化试验期间处于稳定工作状态, 退化模式始终为渐进模式。以输出功率降到初始值的 50% 作为失效判

收稿日期: 2021-06-08; 修回日期: 2021-07-31; 录用日期: 2021-08-17

基金项目: 国家重点研发计划(2018YFB2200601)、中国科学院战略性先导科技专项(B类)(XDB43000000)

通信作者: \*jlxiao@semi.ac.cn

据标准<sup>[14]</sup>,对耦合双圆 WGM 微腔激光器的寿命进行初步的估计。结果表明,在 100 mA 注入电流下,该器件的寿命约为 1200 h。

## 2 器件结构和工艺

电老化试验使用的是半径  $R = 15 \mu\text{m}$  的耦合双圆微腔激光器,器件采用 InGaAsP/InP 多量子阱外延片制作,微腔与波导相切耦合<sup>[15]</sup>。图 1 是激光器

结构的截面示意图,插图是激光器结构的立体示意图,其中 P、N 为掺杂类型,p、n 为电极类型。该器件使用  $\text{SiO}_2$  掩膜完成对腔体的深刻蚀:采用等离子体增强化学气相沉积技术在外延片上沉积厚度为 800 nm 的  $\text{SiO}_2$  层,用标准光刻和感应耦合等离子体(ICP)刻蚀技术将图形转移到  $\text{SiO}_2$  层,以图形化  $\text{SiO}_2$  为掩膜对外延片进行 ICP 刻蚀,刻蚀深度为  $6 \mu\text{m}$ ,用化学腐蚀的方法提高了刻蚀侧壁的光滑性。

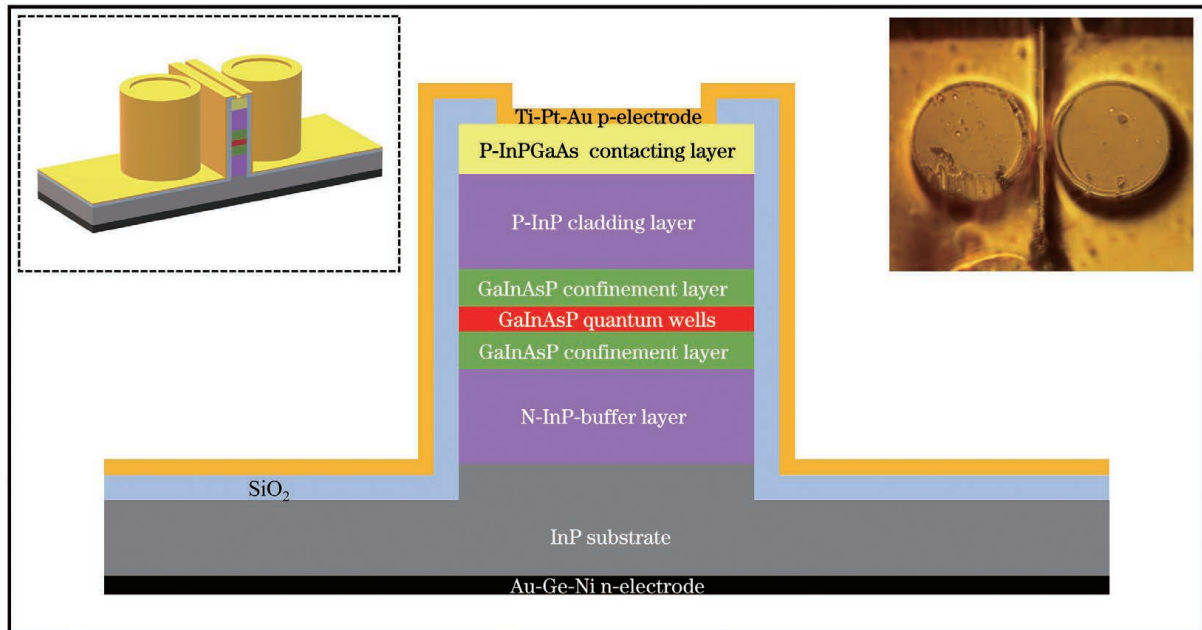


图 1 耦合双圆微腔激光器的结构示意图

Fig. 1 Structural diagram of coupled-circular micro-cavity laser

这种深刻蚀结构实现了光在腔体内部的全反射,为了确保侧向的强限制和纵向泄漏到衬底的光尽量少,要求刻蚀超过有源区,对上下光限制层均进行刻蚀,并根据外延结构各层的折射率及厚度,通过时域有限差分方法对刻蚀深度进行优化设计。但深刻蚀给有源区部分的刻蚀界面带来了大量的缺陷和损伤,特别是非辐射复合中心。缺陷和位错的生长是造成有源区退化的典型原因,注入电流(电子和空穴)、注入电流和周围环境产生的热量及发射光会加速缺陷和位错的生长。因此,WGM 的深刻蚀结构对激光器可靠性的影响可以分为三方面。首先,工作中激光器的有源区内部发生辐射复合以及非辐射复合,辐射复合释放的光子被非辐射复合中心吸收,形成暗斑缺陷,非辐射复合释放的声子转化为晶格振动,产生低温缺陷运动,有源层中开始产生螺旋位错,形成位错偶极子,位错网络从有源层中的位错偶极子处延伸,产生暗线缺陷。其次,刻蚀界面吸收非辐射复合释放的能量,温度升高,非辐射复合中心增

加,产热变多,进一步促使缺陷增加。另外,WGM 微腔刻蚀界面处的光场强度较高,会加速缺陷和损伤的发展。因此,这种特殊的深刻蚀结构会加速 WGM 微腔激光器的退化。

WGM 微腔刻蚀侧壁的形貌直接影响光在腔面上的反射,对腔内模式限制至关重要。刻蚀界面的粗糙度越大,除了带来越严重的散射损耗外,引入的缺陷和损伤也越多,从而影响激光器的寿命;刻蚀界面的陡直度差,会造成模式品质因子的大幅下降。因此,这种深刻蚀结构对工艺的要求非常高。为了提高刻蚀侧壁的陡直度和平滑度,可以通过如下方法实现。

1) 掩膜层的选择。对于 InP 系半导体材料,常用的掩膜包括光刻胶、金属、 $\text{SiO}_2$  和  $\text{SiN}_x$  等。普通光刻胶在离子轰击下会焦化变形,不适合应用于 ICP 深刻蚀中,金属掩膜又容易对刻蚀腔室造成污染。 $\text{SiO}_2$  与 InP 系半导体黏附性好且容易用 HF 溶液直接去除,因此本文选用  $\text{SiO}_2$  作掩膜层,

结合 ICP 刻蚀技术来完成深刻蚀。

2) 优化 ICP 刻蚀气体等刻蚀条件。采用刻蚀气体 Ar、Cl<sub>2</sub> 和 CH<sub>4</sub>, 可以精确控制刻蚀深度, 但刻蚀选择比较低; 采用刻蚀气体 H<sub>2</sub> 和 Cl<sub>2</sub>, 刻蚀速率快, 刻蚀陡直度好, 刻蚀选择比高, 但精确控制刻蚀深度的难度较大。在实际器件制备过程中, 使用的刻蚀气体是 Cl<sub>2</sub>、CH<sub>4</sub> 和 H<sub>2</sub>。

3) 通过 InP 干法刻蚀后, 结合饱和溴水进行湿法腐蚀以提高侧壁的光滑度。

### 3 电老化试验和性能测试

在电老化试验进行前, 要对选定的器件进行筛查, 防止选中的器件性能不稳定, 在试验早期退化失效。首先对器件进行目检, 然后测试其功率-电压-电流 ( $P$ - $V$ - $I$ ) 特性, 保证器件能够正常工作。对通

过筛查的微腔激光器进行恒电流模式的电老化试验, 电流应力为 100 mA, 老化总时长为 1400 h。利用单模光纤收集输出光。所有测试均在室温大气环境下进行, 试验期间环境温度变化范围为 18 ~ 26 °C, 湿度变化范围为 9% ~ 34%。

在电老化试验的前期 (第 20 h)、中期 (第 400 h) 和后期 (第 1250 h), 环境温度均为 20 °C。注入电流  $I=100$  mA 时, 第 20, 400, 1250 h 激光器的输出光谱如图 2(a) 所示, 可以看到激射模式在 1523 nm 附近, 表现为多峰结构。双圆谐振腔的工艺误差导致了模式波长的细小差异, 不同谐振波长的叠加导致了多模激射。第 20, 400, 1250 h 激光器的输出功率和电压随注入电流的变化曲线如图 2(b) 所示, 对应的阈值电流分别为 57, 61, 68 mA, 当注入电流  $I=100$  mA 时, 输出功率分别为 3.73, 3.10, 1.77  $\mu$ W。

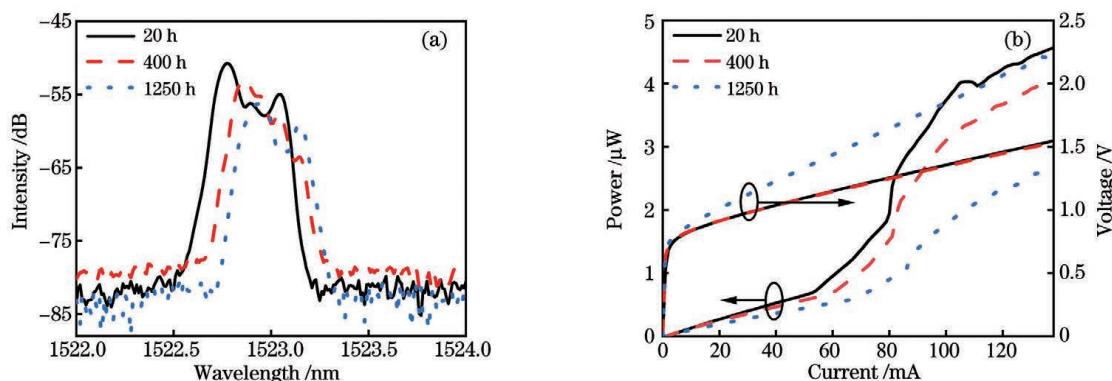


图 2 第 20, 400, 1250 h 激光器的性能。(a)  $I=100$  mA 时的输出光谱; (b)  $P$ - $V$ - $I$  曲线

Fig. 2 Laser characteristics at 20, 400, and 1250 h. (a) Output spectra at  $I=100$  mA; (b)  $P$ - $V$ - $I$  curves

以电老化试验的中期 (第 400 h) 为例, 对微腔激光器的性能进行分析。器件在 1517 nm 附近的激射模式的细致光谱如图 3(a) 所示, 注入电流  $I=130, 135, 140, 145, 150$  mA, 随着注入电流的增大, 激射模式发生红移, 激射波长随注入电流的变化率  $\Delta\lambda/\Delta I$  为 0.0405 nm/mA。通过拟合  $V$ - $I$  曲线, 得

到器件的串联电阻约为 5.14  $\Omega$ 。  $I=130$  mA 时微腔激光器的光谱如图 3(b) 所示, 可以看到纵模间距约为 7.5 nm, 取群折射率  $n_g$  为 3.44, 纵模间距的试验值与圆形微腔纵模间距  $\lambda^2/(2\pi R n_g)$  的计算值相接近, 其中  $\lambda$  是激射波长。

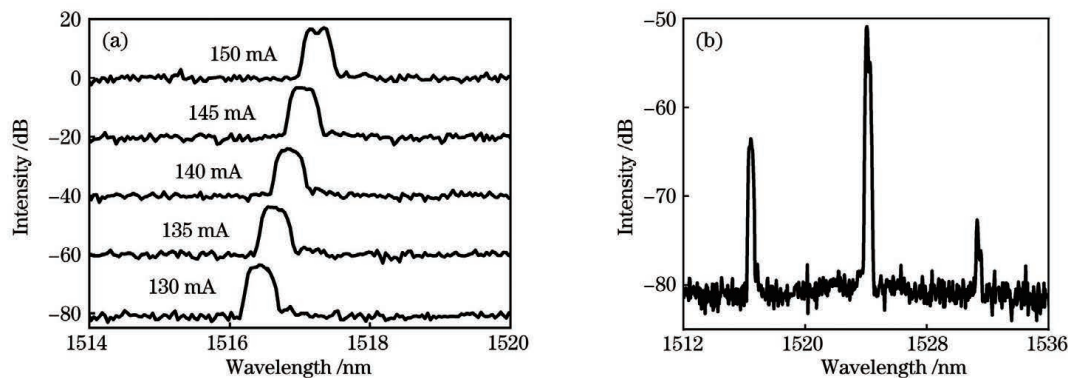


图 3 第 400 h 激光器的输出光谱。(a)  $I=130, 135, 140, 145, 150$  mA 时的细致光谱; (b)  $I=130$  mA 时的光谱

Fig. 3 Laser output spectra at 400 h. (a) Detailed spectra at  $I=130, 135, 140, 145, 150$  mA; (b) spectrum at  $I=130$  mA

在电老化试验期间,微腔激光器的输出功率和阈值电流随时间的变化曲线如图 4 所示,环境温度的变化作为重要的影响因素也绘制在图中。可以看

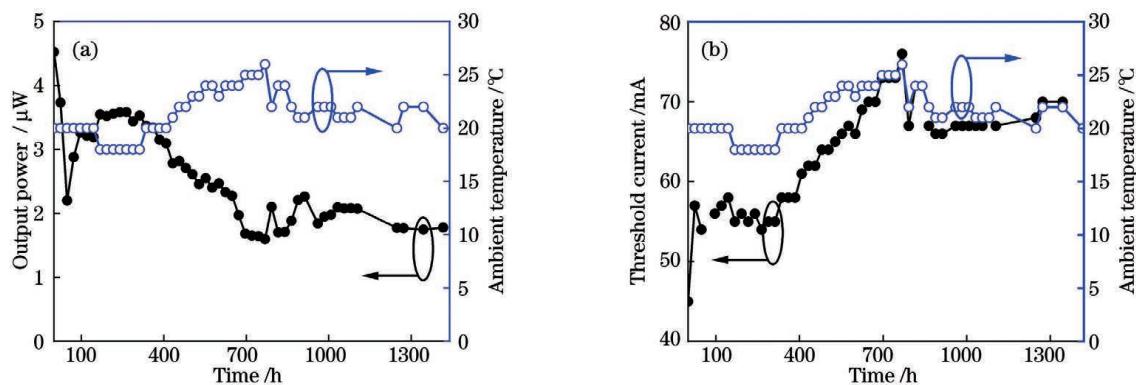


图 4 电老化试验期间激光器的输出功率和阈值电流随时间的变化曲线。(a)  $I=100$  mA 时的输出功率;(b) 阈值电流  
 Fig. 4 Laser output power and threshold current versus time during aging test. (a) Output power at  $I=100$  mA;  
 (b) threshold current

## 4 分析与讨论

根据器件特性的变化率,半导体激光器的退化模式大致可以分为快速退化、渐进退化和灾难退化模式<sup>[16]</sup>。器件保持渐进退化模式不变时,性能退化缓慢,工作状态稳定,处于器件工作性能最佳时期,对器件寿命的评价也要在这个时期内进行。在电老化试验前对器件的外观和  $P$ - $V$ - $I$  特性进行了筛查,但仍要通过分析输出功率和阈值电流的变化曲线来判断试验期间器件的退化模式是否始终为渐进退化模式。如图 4 所示,在电老化试验期间,除 0~100 h 和 670~920 h 范围内输出功率以及 335~820 h 范围内阈值电流的变化情况异常外,输出功率和阈值电流随时间变化的曲线符合渐进退化模式的变化特点,即输出功率呈现不断下降的趋势,且下

到,随着时间的推移,在 100 mA 下,输出功率呈现不断下降的趋势,并且下降速度越来越缓慢,而阈值电流呈现不断上升的趋势。

降速度越来越缓慢,阈值电流呈现不断上升的趋势,且上升速度越来越缓慢。

0~100 h 范围内的输出功率曲线出现异常下降,在此期间环境温度不变,输出光谱如图 5(a) 所示,可以看到,激射模式峰的形态发生了明显的变化,输出功率曲线出现异常下降是由于模式发生了变化。670~920 h 范围内的输出功率曲线出现异常波动,为了研究曲线波动是否是受到了环境温度的影响,计算器件实际有源区温度,并与环境温度的变化趋势进行对比。器件实际有源区温度的计算方法如下。因为器件激射模式明显为多峰结构,所以选取中心波长位置来量化激射模式波长的红移,以第 670 h 为例,激射波长随注入电流的变化曲线如图 5(b) 插图所示。参照激光器激射波长随温度的变化  $\Delta\lambda/\Delta T$  为 0.1 nm/K<sup>[17]</sup>,根据激射波长与注

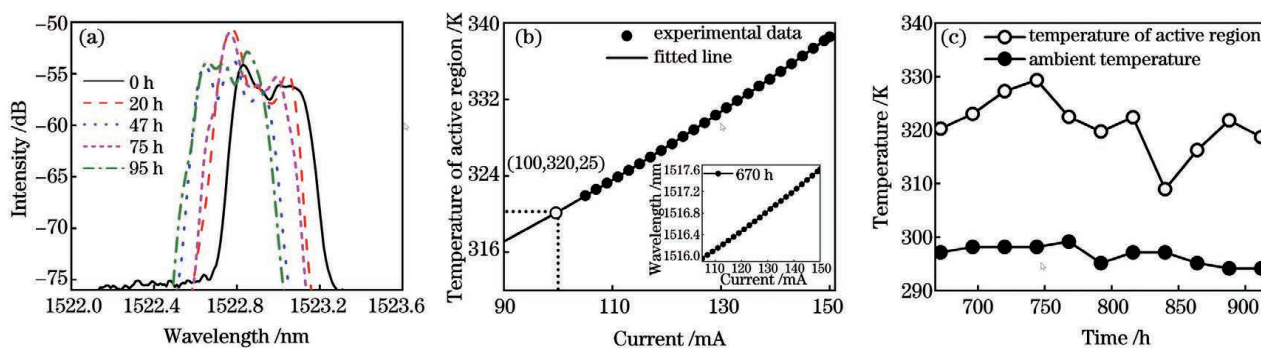


图 5 器件输出功率和阈值电流异常变化的分析。(a)  $I=100$  mA 时激光器的输出光谱;(b) 有源区温度随注入电流的变化曲线,其中插图是激射波长随注入电流的变化曲线;(c)  $I=100$  mA 时温度随时间的变化曲线  
 Fig. 5 Abnormal change analysis of output power and threshold current of device. (a) Laser output spectra at  $I=100$  mA;  
 (b) temperature of active region versus injection current with lasing wavelength versus injection current shown in  
 inset; (c) temperature versus time at  $I=100$  mA

入电流的关系,可以得到不同注入电流下对应的有源区温度,将有源区温度( $T$ )与注入电流的对应关系进行拟合。第 670 h 的拟合结果为  $T=9.01378 \times 10^{-4} I^2 + 0.14087 I + 297.15$ ,如图 5(b)所示,外推计算得到注入电流  $I=100$  mA 时有源区温度为 320.25 K。同理得到 670~920 h 范围内的器件实际有源区温度随时间的变化曲线,如图 5(c)所示,可以看到,该时间段内器件有源区温度与环境温度的变化趋势基本一致,因此输出功率曲线的波动是受到了环境温度的影响。335~820 h 范围内的阈值电流上升速度加快,如图 4(b)所示,这也是环境温度变化导致的。

经过上述分析可知,电老化试验期间输出功率和阈值电流出现异常变化区间是由于模式或环境温度发生了变化,并不是器件退化模式变化造成的,因此该器件在电老化试验期间始终处于渐进退化模式,即试验期间器件处在工作性能最佳时期,输出功率的变化情况可以作为评价该器件寿命的依据。该微腔激光器的输出功率在第 1200 h 左右时降到初始值的 50%,如图 4(a)所示,即以输出功率降到初始值的 50% 作为失效判据标准时,电流应力 100 mA 下器件的寿命约为 1200 h。

## 5 结 论

选取恒电流模式对由边发射 InGaAsP/InP 多量子阱外延片制作的半径为  $R=15 \mu\text{m}$  的耦合双圆 WGM 微腔激光器进行了电老化试验,电流应力为 100 mA。除了模式或环境温度变化导致的异常变化区间外,试验期间输出功率和阈值电流随时间变化的曲线符合渐进退化模式的变化特点,即器件处在工作性能最佳时期,输出功率的变化情况可以作为评价器件寿命的依据。微腔激光器的输出功率在第 1200 h 左右降到初始值的 50%,即 100 mA 电流下器件的寿命约为 1200 h。

研究结果为后续确定 WGM 微腔激光器的早期筛选条件和加速老化条件及搭建老化测试系统等提供了依据。接下来将会针对 WGM 微腔激光器继续开展可靠性研究,对多个器件进行电老化试验。

## 参 考 文 献

- [1] Waters R G. Diode laser degradation mechanisms: a review[J]. Progress in Quantum Electronics, 1991, 15(3): 153-174.
- [2] Souto J, Pura J L, Jiménez J. Microscopic degradation and failure processes in high-power diode lasers[C]//2019 IEEE High Power Diode Lasers and Systems Conference (HPD), October 9-10, 2019, Coventry, UK. New York: IEEE Press, 2019: 13-14.
- [3] Lu G G, Lai G X, Yao B. Evaluation and failure mechanism of high power semiconductor laser packaging[C]//2018 19th International Conference on Electronic Packaging Technology (ICEPT), August 8-11, 2018, Shanghai, China. New York: IEEE Press, 2018: 1671-1674.
- [4] Sun T Y, Xia M J, Qiao L. Research progress of failure mechanism and detection analysis of semiconductor laser [J]. Laser & Optoelectronics Progress, 2021, 58(19): 1900003.  
孙天宇, 夏明俊, 乔雷. 半导体激光器失效机理与检测分析研究进展 [J]. 激光与光电子学进展, 2021, 58(19): 1900003.
- [5] Chen L H, Yang G W, Liu Y X. Development of semiconductor lasers[J]. Chinese Journal of Lasers, 2020, 47(5): 0500001.  
陈良惠, 杨国文, 刘育衍. 半导体激光器研究进展 [J]. 中国激光, 2020, 47(5): 0500001.
- [6] Lu G G, Xie S F, Hao M M, et al. High power diode lasers reliability experiment[J]. Proceedings of SPIE, 2013, 9042: 90421H.
- [7] McCall S L, Levi A F J, Slusher R E, et al. Whispering-gallery mode microdisk lasers[J]. Applied Physics Letters, 1992, 60(3): 289-291.
- [8] Yao Z S, Wu K Y, Tan B X, et al. Integrated silicon photonic microresonators: emerging technologies[J]. IEEE Journal of Selected Topics in Quantum Electronics, 2018, 24(6): 1-24.
- [9] Liao M L, Huang Y Z, Weng H Z, et al. Narrowlinewidth microwave generation by an optoelectronic oscillator with a directly modulated microsquare laser [J]. Optics Letters, 2017, 42(21): 4251-4254.
- [10] Han J H, Park S W. Wafer level reliability and lifetime analysis of InGaAsP/InP quantum-well Fabry-Pérot laser diode [J]. IEEE Transactions on Device and Materials Reliability, 2005, 5(4): 683-687.
- [11] Huang J S. Reliability-extrapolation methodology of semiconductor laser diodes: is a quick life test feasible? [J]. IEEE Transactions on Device and Materials Reliability, 2006, 6(1): 46-51.
- [12] Liu Q K, Kong J X, Zhu L N, et al. Failure mode analysis of high-power laser diodes by electroluminescence[J]. Chinese Journal of Luminescence, 2018, 39(2): 180-187.  
刘启坤, 孔金霞, 朱凌妮, 等. 电致发光用于大功率

- 半导体激光器失效模式分析[J]. 发光学报, 2018, 39(2): 180-187.
- [13] Yuan Q H, Jing H Q, Zhong L, et al. High-power and high-reliability 9XX-nm laser diode[J]. Chinese Journal of Lasers, 2020, 47(4): 0401006.
- 袁庆贺, 井红旗, 仲莉, 等. 高功率高可靠性 9XX nm 激光二极管[J]. 中国激光, 2020, 47(4): 0401006.
- [14] Lu G G, Tao G T, Yao S, et al. Accelerated aging of 808 nm high-power semiconductor laser diodes[J]. Semiconductor Optoelectronics, 2005, 26(2): 97-99.
- 路国光, 套格套, 尧舜, 等. 808 nm 大功率半导体激光器的加速老化实验[J]. 半导体光电, 2005, 26(2): 97-99.
- [15] Lin J D, Huang Y Z, Yang Y D, et al. Optical bistability in GaInAsP/InP coupled-circular resonator microlasers[J]. Optics Letters, 2011, 36(17): 3515-3517.
- [16] Ueda O. Degradation of III-V opto-electronic devices [J]. Journal of the Electrochemical Society, 1988, 135(1): 11C-22C.
- [17] Lü X M, Zou L X, Lin J D, et al. Unidirectional-emission single-mode AlGaInAs-InP microcylinder lasers [J]. IEEE Photonics Technology Letters, 2012, 24(11): 963-965.

## Electrical Aging Test and Lifetime Analysis of Whispering-Gallery-Mode Micro-Cavity Lasers

Fan Yingrun<sup>1,2</sup>, Xiao Jinlong<sup>2,3\*</sup>, Yang Yuede<sup>2,3</sup>, Hao Youzeng<sup>2,3</sup>, Huang Yongtao<sup>2,3</sup>, Huang Yongzhen<sup>1,2,3</sup>

<sup>1</sup> School of Microelectronics, University of Chinese Academy of Sciences, Beijing 100049, China;

<sup>2</sup> State Key Laboratory of Integrated Optoelectronics, Institute of Semiconductors, Chinese Academy of Sciences, Beijing 100083, China;

<sup>3</sup> Center of Materials Science and Optoelectronics Engineering, University of Chinese Academy of Sciences, Beijing 100049, China

### Abstract

**Objective** Whispering-gallery-mode (WGM) semiconductor micro-cavity lasers have the characteristics of small sizes, high quality factors, and easy integration, and have a wide range of potential applications in on-chip photonic integration, microwave photonics and other fields. Semiconductor lasers will degrade and even fail due to catastrophic optical damages, facet oxidation, electrostatic damages and degradation of electrodes and bonds in operation, which influence the reliability of their application systems. Especially, the WGM micro-cavity adopts the deep etching structure etched through active layers, different from other laser cavities. The deep etching structure is used to realize total internal reflection at the dielectric boundary with a high-low refractive index contrast for a small bending radius, but it also brings a lot of defects and damages to the etching interface including the active layer, especially the non-radiative recombination centers. The non-radiative recombination centers absorb the photons released in the radiative recombination process and become the dark spot defects. The energy emitted by the non-radiative recombination is transformed into lattice vibrations through phonon emission and can give rise to the low-temperature defect motion. Thus the dislocations in the active layer begin to be generated and deformed. Simultaneously, the etching interface absorbs the energy emitted by the non-radiative recombination, its temperature rises and defects increase. The generated heat becomes more and further promotes the increase of defects. The high optical field intensity at the etching interface of WGM micro-cavity laser will also accelerate the expansion of defects and damage. Therefore, the deep etching structure accelerates the degradation of WGM micro-cavity lasers. In order for them to work stably in their application system, it is necessary to study the reliability of WGM micro-cavity lasers that has not been studied before, and to examine their lifetime at optimum operating conditions.

**Methods** In order to analyze the lifetime of WGM semiconductor micro-cavity lasers, the InGaAsP/InP multiple-quantum-well coupled-circular micro-cavity laser is measured by the constant current aging test at 100 mA for 1400 h. The constant current aging test requires only measuring the output power under a constant current at an interval of several hours or days. Before the aging test, the selected laser should be screened to prevent performance instability, degradation or failure in the early stage of the aging test. The appearance of the laser needs to be

checked, including its structure, morphology, and etching depth. The power-voltage-current ( $P$ - $V$ - $I$ ) characteristics are also investigated to determine whether the laser is on or leaked. The value of inflection point of the  $V$ - $I$  curve, i. e. threshold voltage, should be about 0.7 V. The  $P$ - $V$ - $I$  curve and output spectrum of the laser are measured every 24 h. During the aging test, the ambient temperature varies from 18 °C to 26 °C.

**Results and Discussions** During the aging test, the output power and threshold current of the micro-cavity laser versus time are shown in Fig. 4, and the change of ambient temperature, as an important influence factor, is also plotted in this figure. The output power decreases more and more slowly, and the threshold current increases more and more slowly during the aging test, except the output power changes abnormally in 0–100 h and 670–920 h, and the threshold current changes abnormally in 335–820 h. The lifetime of the micro-cavity laser can only be evaluated when the laser is under the gradual degradation mode, in which the performance degrades slowly and the working state is stable. The variations of the output power and threshold current of the laser during the test are consistent with those of the semiconductor laser under the gradual degradation mode, except for the three abnormal variations in 0–100 h, 670–920 h, and 335–820 h. As shown in the output spectrum in Fig. 5(a), the shape of the mode peak changes obviously at a constant ambient temperature in 0–100 h, so the abnormal decrease of the output power is affected by the mode change. According to the lasing wavelength curve versus injection current at 670 h, the active region temperatures at different injection currents are obtained. By fitting and extrapolation calculation, the active region temperature at 100 mA is 320.25 K, as shown in Fig. 5(b). Similarly, the active region temperature in 670–920 h is obtained, as shown in Fig. 5(c). The change of the active region temperature is consistent with that of the ambient temperature except for the change at the 840 h, so the abnormal variation of the output power is affected by the ambient temperature in 670–920 h. Similarly, the abnormal increase of threshold current is also caused by the change of ambient temperature in 335–820 h. Therefore, the three abnormal variations of the output power and threshold current are due to the change of mode or ambient temperature, rather than the change of the degradation mode. So the laser is always under the gradual degradation mode during the aging test, and the lifetime of the laser can be evaluated according to the variation of output power. The output power of the laser is reduced by 50% after 1200 h, that is, the lifetime of the laser is about 1200 h at 100 mA, as shown in Fig. 4(a).

**Conclusions** The InGaAsP/InP multiple-quantum-well coupled-circular micro-cavity laser with a radius of 15  $\mu\text{m}$  is measured by the constant current aging test at 100 mA for 1400 h. The variations of laser output power and threshold current during the test are consistent with those of a semiconductor laser under the gradual degradation mode except for three abnormal variations caused by the change of mode or ambient temperature, that is, the lifetime of the laser can be evaluated according to the output power variation. The laser output power is reduced by 50% after 1200 h, that is, the lifetime of the laser is about 1200 h at 100 mA.

**Key words** lasers; micro-cavity; reliability; electrical aging test; current stress; lifetime